An Isolated Single-Switch ZCS Resonant Converter With High Step-Up Ratio

Jaeyeon Lee, Minjae Kim, Sunju Kim, and Sewan Choi, *Fellow, IEEE*

***Abstract*—This article proposes an isolated high step-up resonant converter which is suitable for low power application. The proposed converter is simple in structure since it employs only one switch while not necessitating a clamp circuit. Also, the proposed converter is able to achieve ZCS turn-ON and turn-OFF of the switch and ZCS turn-OFF of diodes using a parallel resonant circuit, resulting in high efficiency. Furthermore, the proposed converter has reduced transformer volume due to zero dc-offset current in transformer. Experimental results on 450-W prototype are provided to validate the proposed concept.**

***Index Terms*—High step-up, resonant converter, single switch, soft switching.**

I. Introduction

In THE renewable energy systems, such as photovoltaic module-integrated converter systems, fuel cell systems, hybrid electric vehicles, and uninterruptible power systems, high power density, high efficiency, and low cost dc–dc converters have been required [1]–[4]. Generally, these systems are composed of a dc–dc converter usually with low and wide input voltage and a dc–ac inverter. In order to boost the low input voltage to a high output voltage of the dc link terminal, a high step-up converter is required at the dc–dc stage. In the applications that require high step-up output voltage, the isolated topologies are preferable because they can achieve higher efficiency than the nonisolated converters by properly designing the transformer's turn ratio. Moreover, the transformer provides galvanic isolation between the input and output, which is desired from the safety perspective [5]–[8].

A number of isolated dc–dc converters have been proposed for high step-up applications [9]–[27]. The isolated high step-up dc–dc converter has two kinds of topologies: passive clamp converters [9], [10] and active clamp converters [11]–[19]. The passive clamp converters have simple structure and low switch count, but suffers from considerable power losses associated with hard switching of main switch. Besides, the RCD snubber circuit of the passive clamp converter causes large amount of losses. The active clamp converters have actively been developed based on three basic topologies: push–pull [11]–[13], half-bridge [14]–[16], and full-bridge [17]–[19]. These active clamp converters not only achieve zero-voltage switching (ZVS) turn-ON of switches but eliminate the voltage spike that is induced by the trapped energy in the leakage inductor of the transformer with the help of the active clamp, thereby being able to further increase switching frequency. However, it seems not to obtain high efficiency and low cost in low power application due to many switches and their driving circuits.

In response to this concern, single switch isolated dc–dc converters have been proposed for low power applications [20]–[27]. Single switch isolated dc–dc converters could be PWM converters [20]–[23] such as Z-source converter and flyback converter or resonant converters [24]–[26] such as CL, LCL, and CLL resonant converter. The Z-source [20] and flyback converters [21] have only one switch and one clamp circuit, but the switch is hard switched at both turn-ON and turn-OFF instants. Frequency-controlled flyback converter [22] and series-connected forward-flyback converter [23] achieve zero-current switching (ZCS) turn-ON of switch, but the switch is hard switched at turn-OFF instant. In contrast, resonant converters [24]–[26] have many advantages such as the followings: 1) soft switching turn-ON and turn-OFF of switch; 2) utilization of parasitic elements such as leakage and/or magnetizing inductor of transformer as resonant elements; and 3) simple structure due to absence of clamp circuits. However, the aforementioned single switch topologies have large dc-offset current in the transformer leading to increase transformer volume. The electrolytic capacitor-less converter [27] can reduce the transformer volume due to low magnetizing current. Besides, the converter achieves not only ZVS turn-ON of switch, but also ZCS turn-OFF of switch. But, in order to achieve the high step-up ratio, the operation switching frequency range should be wide enough to accommodate variations in input.

In this article, a single switch ZCS resonant converter is proposed for isolated high step-up application. The proposed converter was previously presented in the conference [28], [29] with the discussion of simulation results. The proposed converter has the following features:

1) reduced transformer volume due to zero dc-offset current in transformer;
2) simple structure due to absence of clamp circuits;
3) ZCS turn-ON and turn-OFF of switch regardless of voltage and load variation.

Manuscript received January 14, 2021; revised March 20, 2021; accepted April 3, 2021. Date of publication April 13, 2021; date of current version June 30, 2021. This work was supported by the National Research Foundation of Korea (NRF) grant funded by the Korea Government (MSIT) under Grant 2020R1A2C2006301. Recommended for publication by Associate Editor J. Lam. *(Corresponding author: Sewan Choi.)*

The authors are with the Department of Electrical and Information Engineering, Seoul National University of Science and Technology, Seoul 01811, South Korea (e-mail: wodus847@seoultech.ac.kr; tostood@seoultech.ac.kr; rlatjswn831@seoultech.ac.kr; schoi@seoultech.ac.kr).

Color versions of one or more figures in this article are available at https://doi.org/10.1109/TPEL.2021.3072647.

Digital Object Identifier 10.1109/TPEL.2021.3072647

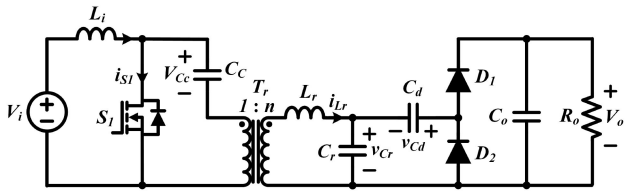

Fig. 1. Circuit diagram of the proposed converter.

4) ZCS turn-OFF of all diodes leading to negligible voltage surge associated with the diode reverse recovery;
5) high-voltage gain within narrow operation switching frequency range.

These features make it possible to achieve high efficiency and low cost in the low power, high step-up application. Experimental results on 450-W prototype are provided to validate the proposed concept.

II. Proposed Single Switch Converter

Fig. 1 shows the circuit diagram of the proposed converter; it consists of input filter L_i, switch S_1, clamp capacitor C_C at the transformer primary side, and L_r–C_r parallel resonant tank and voltage doubler rectifier at the transformer secondary side. The output voltage of the proposed converter is regulated by switching frequency variation.

A. Operating Principle

Figs. 2 and 3 show key waveforms and operation states of the proposed converter, respectively. In order to simplify the analysis of the steady-state operation, it is assumed that the input filter inductance is large enough so that it can be treated as a constant current source during a switching period. It is also assumed that C_C, C_d, and C_o are large enough so that they can be treated as constant voltage sources during a switching period. The average voltage across C_C is the same as the input voltage V_i. The operation states of the proposed converter are described as follows.

Mode 1 ($t_0 \sim t_1$): This mode begins when switch S_1 is turned ON at t_0. Then, current i_{Lr} decreases linearly and can be expressed by

$$i_{Lr}(t) = \frac{I_{Li}}{n} - \frac{nV_i + V_o - V_{Cd}}{L_r}(t - t_0), \qquad t_0 < t < t_1. \tag{1}$$

This leads to ZCS turn OFF of diode D_1. The switch current also increases linearly, making switch S_1 to be turned ON with ZCS. This mode ends when current i_{Lr} reaches 0 A.

Mode 2 ($t_1 \sim t_2$): This mode begins when current i_{Lr} changes its directions. Since diode D_2 is reverse biased, L_r and C_r start resonating with the equivalent circuit shown in Fig. 4 (a). The voltage and current of resonant components are determined, respectively, as follows:

$$i_{Lr}(t) = (-nV_i - V_o + V_{Cd})\sqrt{\frac{C_r}{L_r}}\sin(\omega_r(t - t_1)),$$
$$t_1 < t < t_2 \tag{2}$$

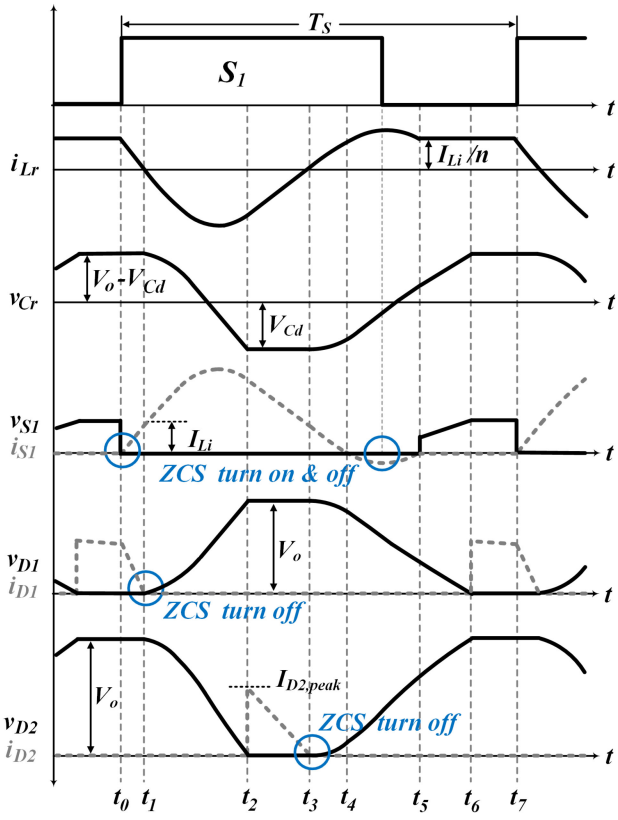

Fig. 2. Key waveforms of the proposed single switch converter.

$$v_{Cr}(t) = (nV_i + V_o - V_{Cd})\cos(\omega_r(t - t_1)) - nV_i,$$
$$t_1 < t < t_2 \tag{3}$$

where $\omega_r = 1/\sqrt{L_r C_r}$. The resonant operation continues until voltage v_{Cr} becomes equal to $-V_{Cd}$.

Mode 3 ($t_2 \sim t_3$): Diode D_2 is turned ON at t_2 when v_{Cr} reaches $-V_{Cd}$. Then, current i_{Lr} decreases linearly and can be expressed by

$$i_{Lr}(t) = i_{Lr}(t_2) - \frac{nV_i - V_{Cd}}{L_r}(t - t_2), \qquad t_2 < t < t_3. \tag{4}$$

This leads to ZCS turn-OFF of diode D_2. This mode ends when current i_{Lr} reaches 0 A.

Mode 4 ($t_3 \sim t_4$): This mode begins when current i_{Lr} changes its directions at t_3. Since diode D_1 is reverse biased, L_r and C_r start resonating with equivalent circuit shown in Fig. 4(b). The voltage and current of resonant components are determined, respectively, as follows:

$$i_{Lr}(t) = (-nV_i + V_{Cd})\sqrt{\frac{C_r}{L_r}}\sin(\omega_r(t - t_3)), \qquad t_3 < t < t_5 \tag{5}$$

$$v_{Cr}(t) = (nV_i - V_{Cd})\cos(\omega_r(t - t_3)) - nV_i, \qquad t_3 < t < t_5. \tag{6}$$

This mode ends when current i_{Lr} reaches I_{Li}/n.

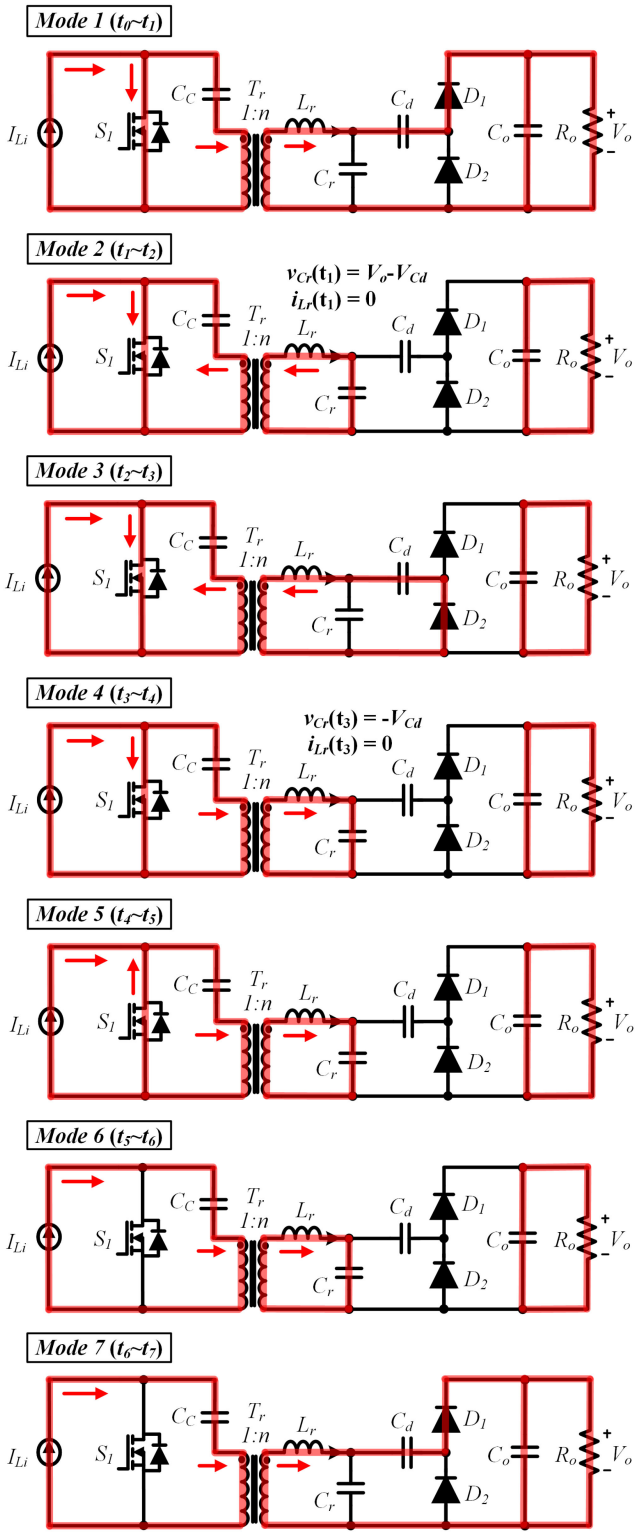

Fig. 3. Operation states of the proposed converter.

Mode 5 ($t_4 \sim t_5$): At time t_4, the current through switch S_1 changes its direction, flowing through main channel of switch S_1 since the gating signal for switch S_1 is still applied. The current flows through the body diode of switch S_1 when switch S_1 is turned OFF. It is noted that switch S_1 is turned OFF with ZCS due

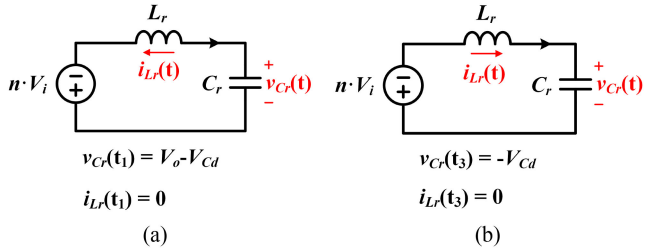

Fig. 4. Equivalent resonant circuits. (a) Mode 2. (b) Modes 4 and 5.

to the L_r–C_r resonance. The resonant operation continues until current i_{Lr} becomes again equal to I_{Li}/n.

Mode 6 ($t_5 \sim t_6$): During this mode, switch S_1 is in the turn-OFF state and the constant current flows through the primary winding of the transformer. Voltage v_{Cr} increases linearly and can be expressed by

$$v_{Cr}(t) = \frac{I_{Li}}{nC_r}(t - t_5) + v_{Cr}(t_5), \qquad t_5 < t < t_6. \tag{7}$$

This mode continues until voltage v_{Cr} reaches V_o–V_{Cd}.

Mode 7 ($t_6 \sim t_7$): At time t_6, diode D_1 is turned ON and the input power is transferred to the output side. This mode ends when switch S_1 is turned ON at time t_7.

B. Voltage Gain Expression

To obtain voltage gain of the proposed converter, voltages across C_C and C_d are assumed to be constant.

From Fig. 2, we have

$$t_7 - t_0 = T_s. \tag{8}$$

The time interval from t_0 to t_1 in Fig. 2 can be obtained from (1) by

$$t_1 - t_0 = \frac{I_{Li}L_r}{n(nV_i + V_o - V_{Cd})}. \tag{9}$$

The time interval from t_1 to t_2 in Fig. 2 can be obtained from (3) by

$$t_2 - t_1 = \frac{1}{\omega_r}\arccos\left(\frac{nV_i - V_{Cd}}{nV_i + V_o - V_{Cd}}\right). \tag{10}$$

Since the average current of diode D_2 is identical to the average load current in the steady state, the following equation is obtained:

$$I_{D2,\text{avg}} = \frac{V_o}{R_o} = \frac{1}{2}I_{D2,\text{peak}}(t_3 - t_2)/T_s. \tag{11}$$

From (4), we have

$$\frac{V_{Cd} - nV_i}{L_r} = \frac{I_{D2,\text{peak}}}{t_3 - t_2}. \tag{12}$$

From (11) and (12), current $I_{D2,\text{peak}}$ can be obtained by

$$I_{D2,\text{peak}} = \sqrt{\frac{2V_o(V_{Cd} - nV_i)}{R_o L_r f_s}}. \tag{13}$$

Applying trigonometric function to (2), (3), and (13), voltage V_{Cd} can be obtained by

$$V_{Cd} = nV_i + \frac{R_o f_s C_r V_o}{2(1 + R_o f_s C_r)}. \tag{14}$$

The time interval from t_2 to t_3 in Fig. 2 can be obtained from (12) and (13) by

$$t_3 - t_2 = \sqrt{\frac{2V_o L_r}{R_o f_s (V_{Cd} - nV_i)}}. \tag{15}$$

The time interval from t_3 to t_5 in Fig. 2 can be obtained from (5) by

$$t_5 - t_3 = \frac{\pi}{\omega_r} - \frac{1}{\omega_r} \arcsin\left(\frac{I_{Li}}{n(V_{Cd} - nV_i)}\sqrt{\frac{L_r}{C_r}}\right). \tag{16}$$

Since the average current of diode D_1 is identical to the average load current in the steady state, the following equation is obtained:

$$t_6 - t_5 = \frac{nC_r}{I_{Li}}\left(V_o - V_{Cd} + nV_i - \sqrt{(V_{Cd} - nV_i)^2 - \frac{L_r}{C_r}\left(\frac{I_{Li}}{n}\right)^2}\right). \tag{17}$$

Since the average current of diode D_1 is identical to the average load current in the steady state, the following equation is obtained:

$$I_{D1,\text{avg}} = \frac{V_o}{R_o} = \frac{I_{Li}}{2n}\left((t_1 - t_0) + 2(t_7 - t_6)\right)/T_s. \tag{18}$$

The time interval from t_6 to t_7 in Fig. 2 can be obtained from (9) and (18) by

$$t_7 - t_6 = \frac{nV_o T_s}{R_o I_{Li}} - \frac{I_{Li} L_r}{2n(nV_i + V_o - V_{Cd})}. \tag{19}$$

From (8)–(10), (14)–(17), and (19), the voltage gain can be obtained by (20), as shown at the bottom of next page.

III. Design Guideline

A design example of the proposed converter is presented in this section. The following converter specifications are considered in the design: output voltage $V_o = 380$ V, input voltage $V_i = 38$∼56 V, output power $P_o = 45$∼450 W, and minimum switching frequency $f_{s,\min} = 60$ kHz.

From Fig. 5, converter voltage gain is plotted for different load conditions. The graph has the identical tendency regardless of a turn ratio n. The minimum frequency $f_{s,\min}$ leads to the minimum voltage gain $M_{\min}$ as defined by (21). The resistance at the minimum load is calculated in (22):

$$M_{\min} = \frac{V_o}{V_{i,\max}} \tag{21}$$

$$R_{o,\max} = \frac{{V_o}^2}{P_{o,\min}}. \tag{22}$$

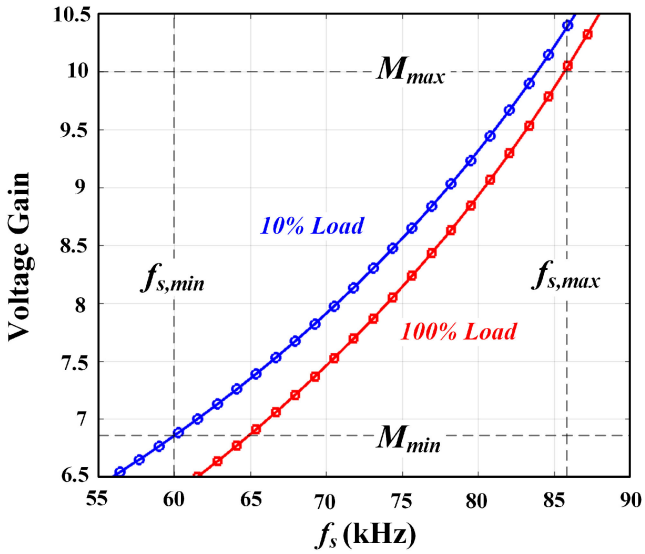

Fig. 5. Voltage gain curves of the proposed converter at different loads ($n = 2$).

Likewise, at $f_{s,\max}$, the maximum voltage gain $M_{\max}$ and the resistance at the maximum load are given as follows:

$$M_{\max} = \frac{V_o}{V_{i,\min}} \tag{23}$$

$$R_{o,\min} = \frac{{V_o}^2}{P_{o,\max}}. \tag{24}$$

Step 1) Determine turn ratio n: Based on the operating principles, the rms current and voltage rating of switch S_1 are calculated, respectively, as follows:

$$I_{S1,\text{rms}} = \sqrt{\frac{1}{T_s}\cdot\int_{t_0}^{t_5}(I_{Li} - n\cdot i_{Lr}(t))^2 dt} \tag{25}$$

$$V_{S1} = \frac{V_o}{2n}\left(1 + \frac{1}{1+k}\right) \tag{26}$$

where $k = R_o C_r f_s$.

Fig. 6 shows rms currents and voltage ratings of switch S_1 based on (25) and (26) for different values of turn ratio n. Regardless of the turn ratio, the resonant inductance L_r range (0∼5μH) is not considered as a category since the switch current rating is very high.

The characteristics of Si MOSFET are very good below voltage rating 150 V. However, a turn ratio equal to 1 is excluded from the selection since the voltage rating is relatively high within the given range. On the other hand, within the design of L_r (18∼23μH), a turn ratio n equal to 2 leads to low switch rms current and voltage rating. A turn ratio n equal to 3 is not considered in the design due to the limited range of L_r (5∼11.5μH). Referring to Fig. 7, a section in the negative direction of the switch current must exist to achieve the soft switching. In other ranges (11.5μH∼), the resonance section is not guaranteed, so

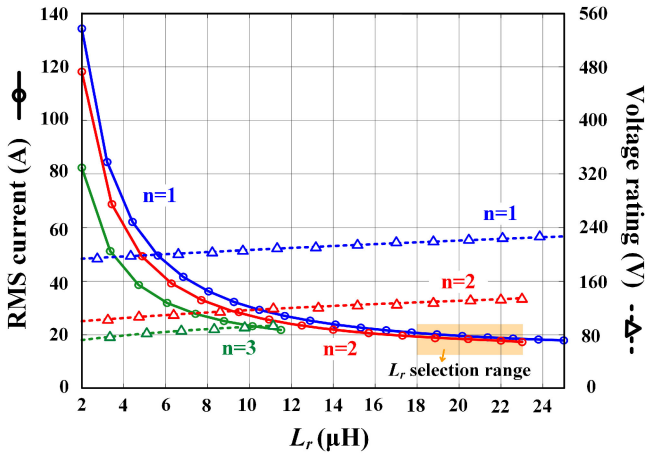

Fig. 6. RMS current and voltage rating of S_1 versus L_r at different n.

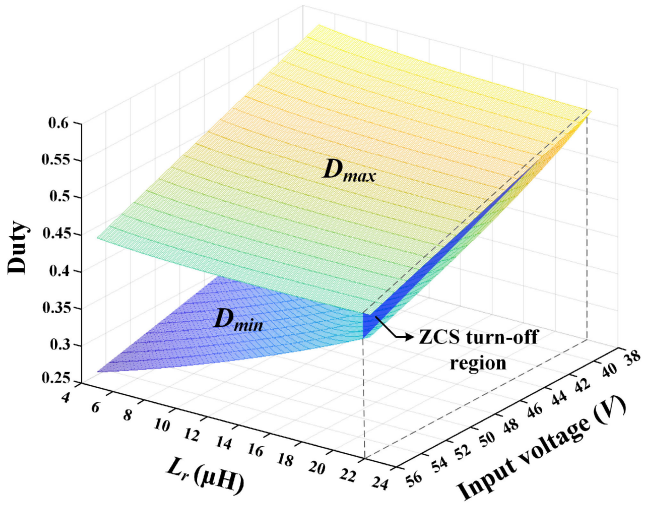

Fig. 8. $D_{\min}$ and $D_{\max}$ versus L_r and input voltage.

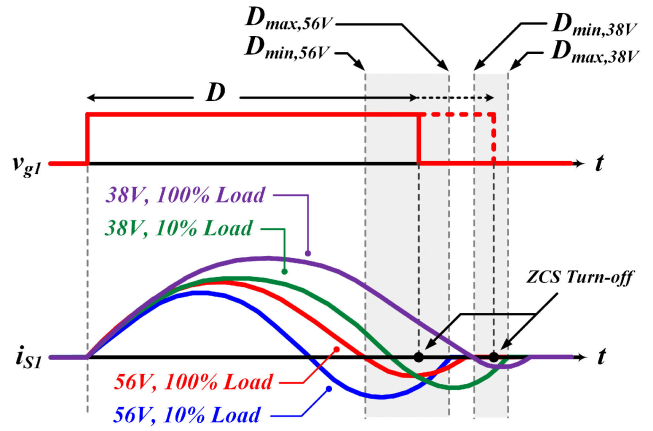

Fig. 7. Gate signal and switch current waveforms for different load conditions at each input voltage.

the switch is hard switched at turn-OFF instant. In addition, the current rating ($n = 3$) is relatively high compared to the resonant inductance selection section (in Fig. 6) at turn ratio equal to 2.

Therefore, the turn ratio n is chosen to be 2 considering the voltage and current rating of switch.

Step 2) Determine L_r and C_r: Fig. 7 shows the concept of switch current waveforms for different load conditions. It is worthy to mention that ZCS turn-OFF is guaranteed for all duty cycles within $D_{\min}$ and $D_{\max}$, *where* $D_{\min}$ is the minimum fixed duty ratio and $D_{\max}$ is the maximum fixed duty ratio, respectively. The $D_{\min}$ and $D_{\max}$ can be obtained from (9), (10), (15), (16) and (21)–(24) by (27) and (28) as shown at bottom of this page, respectively. From (27) and (28), Fig. 8 shows the three-dimensional-plot of $D_{\min}$ and $D_{\max}$ between the resonant value L_r and input voltage V_i. The figure illuminates that the switch is able to achieve the soft switching if the duty value is between the $D_{\max}$ and $D_{\min}$ planes for a given resonant inductance and input voltage value under all load conditions. In this design example, resonant value L_r is chosen to be 22 μH, considering ZCS turn-OFF within entire input voltage range at all load conditions and switch current rating that mentioned in *Step 1* (L_r :18∼23 μH). Using (20)–(22), the

$$M = \frac{V_o}{V_i} = \frac{n\left(k\left(\frac{2+k}{2(1+k)} - \sqrt{\frac{k^2}{4(1+k)^2} - \frac{Z^2M^2}{n^2R_o{}^2}}\right)+1\right)}{\left(1-\frac{L_rMf_s(1+k)}{nR_o(2+k)} + \frac{f_s}{\omega_r}\arccos\left(\frac{k}{2+k}\right) - 2\sqrt{\frac{L_rf_s(1+k)}{R_ok} - \frac{2\pi f_s}{\omega_r} + \frac{f_s}{\omega_r}\arcsin\left(\frac{2MZ(1+k)}{nkR_o}\right)}\right)} \quad (20)$$

where $M = V_o/V_i$, $k = R_oC_rf_s$, $T_s = 1/f_s$ and $Z = \sqrt{L_r/C_r}$

$$D_{\min} = f_{s,\max}\left(\frac{2L_rM_{\max}(1+k_{\min})}{nR_{o,\min}(2+k_{\min})} + \frac{1}{\omega_r}\arccos\left(\frac{-k_{\min}}{2+k_{\min}}\right) + \sqrt{\frac{4L_r(1+k_{\min})}{k_{\min}f_{s,\max}R_{o.\min}}} + \frac{1}{\omega_r}\arcsin\left(\frac{2M_{\max}(1+k_{\min})}{nk_{\min}R_{o,\min}}\sqrt{\frac{L_r}{C_r}}\right)\right)$$

where $k_{\min} = R_{o,\min}C_rf_{s,\max}$ and $\omega_r = \frac{1}{\sqrt{L_rC_r}}$ (27)

$$D_{\max} = f_{s,\min}\left(\frac{2L_rM_{\min}(1+k_{\max})}{nR_{o,\max}(2+k_{\max})} + \frac{1}{\omega_r}\arccos\left(\frac{-k_{\max}}{2+k_{\max}}\right) + \sqrt{\frac{4L_r(1+k_{\max})}{k_{\max}f_{s,\min}R_{o.\max}}} + \frac{\pi}{\omega_r} - \frac{2}{\omega_r}\arcsin\left(\frac{2M_{\min}(1+k_{\max})}{nk_{\max}R_{o,\max}}\sqrt{\frac{L_r}{C_r}}\right)\right)$$

where $k_{\max} = R_{o,\max}C_rf_{s,\min}$ (28)

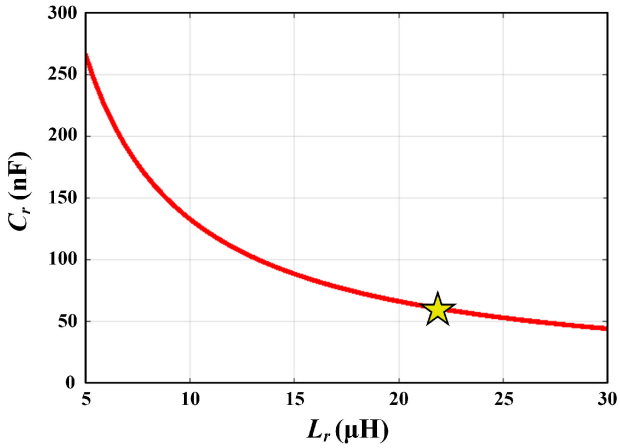

Fig. 9. Relationship between L_r and C_r ($n = 2, f_r = 137$ kHz).

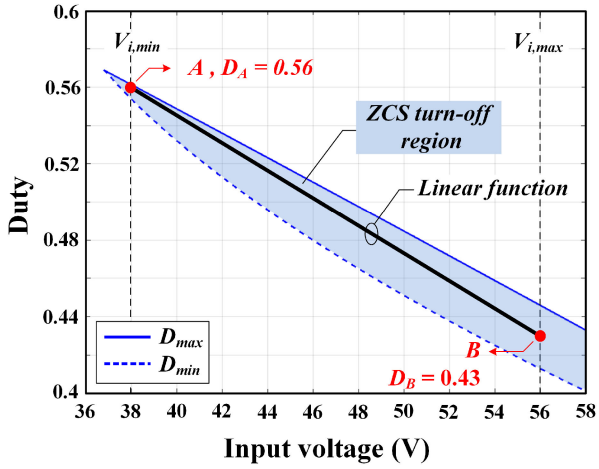

Fig. 10. ZCS turn-OFF region versus V_i under entire load range.

resonant frequency f_r can be calculated that almost equal to 137 kHz, and thus the relationship between resonant value L_r and C_r to meet design specifications can be plotted in Fig. 9. The resonance value C_r corresponding to L_r is 62 nF, which can be selected from Fig. 9.

Step 3) Determine turn-OFF duty D : Fig. 10 is an enlarged the ZCS turn-OFF region in Fig. 8. Likewise, Fig. 10 shows the region that achieves the ZCS turn-OFF under all input voltage ranges and load conditions. To easily find the duty corresponding to the input voltage, a linear function is created by connecting duty point *A* at the minimum voltage and duty *B* at the maximum voltage within the region to achieve ZCS turn-OFF. Then, turn-OFF duty D can be expressed by

$$D = \frac{(D_A - D_B)}{(V_{i,\min} - V_{i,\max})}(V_i - V_{i,\min}) + D_A. \tag{29}$$

IV. Comparative Results

The proposed converter is compared to the recent existing isolated high step-up converters, and the comparison results are summarized in Table I. The Z source converter in [20] has the highest boost ratio and switch utilization, but the switch is turned ON and OFF with hard switching. It is not a major problem that the switch utilization is relatively low since the characteristics of Si MOSFET (voltage rating≤150 V) are very good. Also, the proposed converter is able to achieve ZCS turn-ON and OFF regardless of input voltage and load variation. Note that the soft switching of the proposed converter is achieved by utilizing the resonant elements while not necessitating additional circuit. The isolated converter in [31] is able to achieve not only ZCS turn-ON of switch, but also ZVS turn-OFF of switch. However, it must include a lossless snubber that increases the circuit complexity. Also, in low-power applications, the increase of devices due to additional circuit will be a big issue since adding one or two devices accounts for a large proportion of the total cost. The electrolytic capacitor-less converter in [27] uses one switch and achieves ZVS turn-ON and OFF. However, the efficiency of the converter is relatively low while operating at wide frequency range. The fixed-frequency converter in [32] has the highest efficiency and switching frequency, but uses many switches including four switches at the primary side and two GaN switches at the secondary side. Comparing with the mentioned topologies, the proposed converter is simple since a single switching device is used while operating within narrow frequency range. Moreover, high efficiency is achieved due to maintained soft switching (ZCS turn-ON/OFF) with reduced component count. Therefore, the aforementioned advantages make the proposed isolated single switch converter superior over other counterparts in [20], [27], [31], [32].

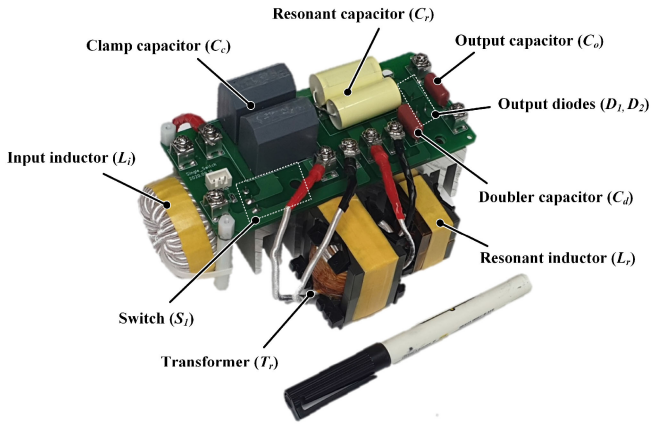

Fig. 11. Prototype of proposed single switch converter.

V. Experimental Results

In order to verify the performance of the proposed single switch converter, a 450-W prototype is built as shown in Fig. 11. The system specification used in the experiment is as follows: $P_o = 450$ W, $V_i = 38{\sim}56$ V, $V_{\rm MPP} = 45$ V $V_o = 380$ V, $n = 2$, $L_r = 22$ μH, and $C_r = 63$ nF. Component ratings and selected devices of the proposed converter are listed in Table II. The control algorithm is implemented in a floating-point DSP platform

TABLE I
COMPARISON WITH OTHER RECENT EXISTING ISOLATED HIGH STEP-UP CONVERTERS

Converter	[20]	[31]	[27]	[32]	Proposed
Gain [V_i/V_o]	16 [25V/400V]	13.5 [28V/380V]	9.5 [40V/380V]	13 [29V/380V]	10 [38V/380V]
Number of Switches	1 [Si]	1 [Si]	1 [Si]	6 [4 Si, 2 GaN]	1 [Si]
Voltage/Current rating of main switch /Switch utilization	$100V_{pk}$/9.5Arms /0.315	$80V_{pk}$/$12.5A_{rms}$ /0.25	$320V_{pk}$/$4A_{rms}$ /0.156	$55V_{pk}$/9.5A_{rms} /0.143	$130V_{pk}$/$18A_{rms}$ /0.192
Number of snubber components / Cost of snubber circuit (excluding inductor)	6 [Passive] /$8.9	4 [Passive] /$4.23	3 [Passive] /$3.3	None	**None**
Switching characteristic (ON/OFF)	Hard switching	ZCS/ZVS	ZVS/ZCS	ZVS/ZCS	ZCS/ZCS
Operation frequency range	50kHz	100kHz	80~150kHz	200kHz	60~86kHz
Efficiency @Rated power	93.5%	96.9%	94%	97.15%	**96.98%**
Maximum power level	300W	250W	200W	300W	450W

TABLE II
PARAMETER'S RATING AND COMPONENTS

Parameters	Rating		Components
Input filter inductor L_i	*Inductance*	300μH	High flux CH400125 (Changsung)
	V_{peak}	90V	
	I_{rms}	11.85A	
Switch S_1	V_{peak}	135V	IRF150P220 (Infineon)
	I_{rms}	18.2A	
Clamp capacitor C_c	*Capacitance*	164μF	FFB44D0826K 2EA, (AVX)
	V_{peak}	56V	
	I_{rms}	11.8A	
Transformer T_r	L_m *Inductance*	68μH	Ferrite core PQ40/40 (TDK)
	Turn ratio	1:2	
Resonant inductor L_r	*Inductance*	22μH	Ferrite core PQ32/30 (TDK)
	V_{peak}	251V	
	I_{rms}	7.4A	
Resonant capacitor C_r	*Capacitance*	63nF	C4CAWUB2330AA0J 2EA, (KEMET)
	V_{peak}	220V	
	I_{rms}	6.1A	
Doubler capacitor C_d	*Capacitance*	1μF	ECQ-E2W105KH (Panasonic)
	V_{peak}	220V	
	I_{rms}	3.9A	
Output diodes D_1 , D_2	V_{peak}	380V	IDH10G65C6 (Infineon)
	I_{avg}	1.2A	
Output capacitor C_o	*Capacitance*	1μF	ECQ-E2W105KH (Panasonic)
	V_{peak}	380V	
	I_{rms}	2.1A	

TMS320F28335. REGATRON AG-Rorschach 9400 is used as a PV simulator device, and ITECH6036C-500-180 is used as a voltage source device that maintains a fixed voltage at the output stage. Also, digital power meter YOKOGAWA WT3000 is used to measure the efficiency. The proposed converter is tested to verify the operating principle, and the experimental results are provided.

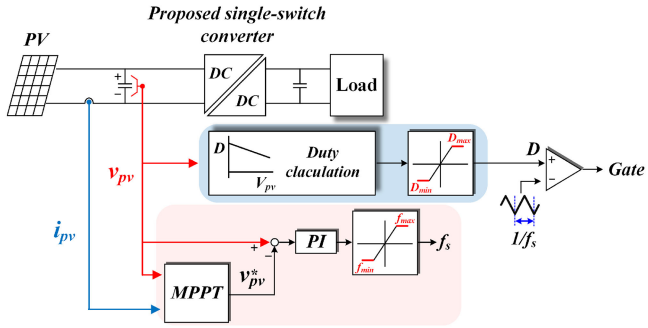

Fig. 12. Control block diagram of the proposed converter.

A. MPPT Implementation

Fig. 12 shows the control block diagram for the proposed converter. The linear function shown in Fig. 10 is applied as the duty ratio to achieve ZCS turn-OFF under all input voltage ranges and load conditions. The PI controller integrates the error between the sensed PV voltage and reference PV voltage to generate the frequency of the proposed converter, and this value is applied as the frequency of the comparator carrier. The P&O MPPT algorithm is applied in the proposed converter and vital for PV applications. To verify the maximum power point tracking, the converter input is connected to the PV power source. When the open circuit voltage is set to 56 V and the maximum power is 450 W, the PV curve is automatically drawn. Meanwhile, the voltage source is connected to the output to clamp the output voltage at 380 V. Fig. 13 shows the experimental voltage and current waveforms of PV source at MPPT. The input voltage at the maximum power point is around 45 V, then the switch is shown to achieve ZCS turn-OFF.

B. Experimental Results

Figs. 14 and 15 show the experimental waveforms of the switch and diodes at full-load and half-load conditions when input voltage is 38 V, respectively. Figs. 14(a) and 15(a) show that switch S_1 is turned ON with ZCS at full-load and half-load conditions. Figs. 14(b) and 15(b) show the voltage and current of switch S_1 that is turned OFF with ZCS at both full-load and

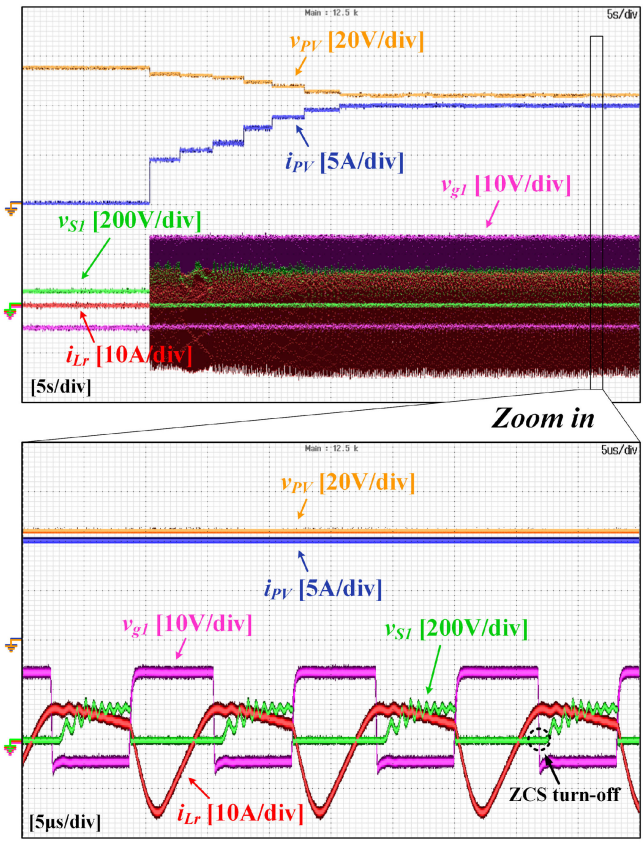

Fig. 13. Experimental waveforms of the maximum power point tracking.

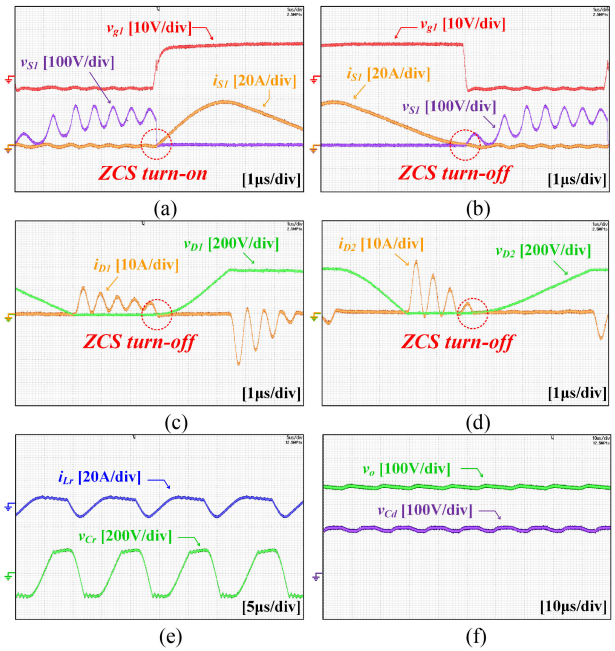

Fig. 14. Experimental waveforms at $V_i = 38$ V and $P_o = 450$ W operation condition. (a) Switch S_1 at turn-ON. (b) Switch S_1 at turn-OFF. (c) Diode D_1 at turn-OFF. (d) Diode D_2 at turn-OFF. (e) Current i_{Lr} and voltage v_{Cr}. (f) Voltage v_o and voltage v_{Cd}.

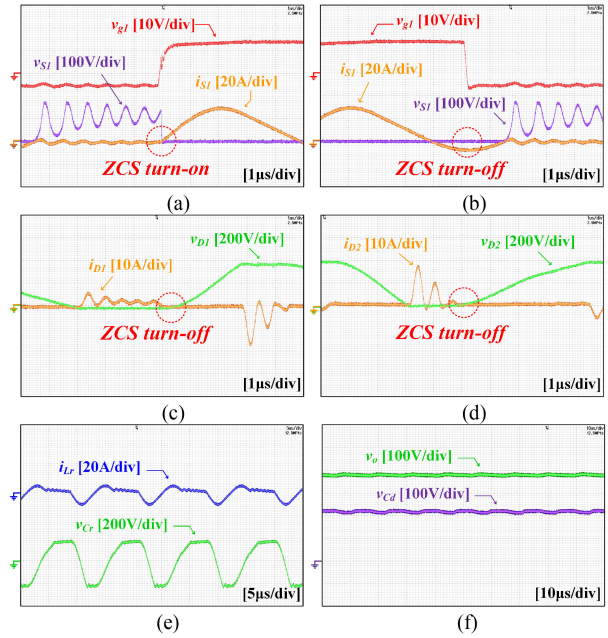

Fig. 15. Experimental waveforms at $V_i = 38$ V and $P_o = 225$ W operation condition. (a) Switch S_1 at turn-ON. (b) Switch S_1 at turn-OFF. (c) Diode D_1 at turn-OFF. (d) Diode D_2 at turn-OFF. (e) Current i_{Lr} and voltage v_{Cr}. (f) Voltage v_o and voltage v_{Cd}.

half-load conditions. Unlike the ideal operating situation, the voltage across the switch has a ringing in Figs. 14(b) and 15(b). The voltage ringing is caused by the parasitic inductance of the PCB board, resonant inductance L_r, and switch output capacitance C_{oss}. This phenomenon is varied widely according to the quality of PCB routing. However, no matter how much the PCB parasitic inductance is reduced, the voltage ringing inevitably occurs due to the resonant inductance L_r and switch output capacitance C_{oss}. Figs. 14(c) and 15(c) show that diode D_1 is turned OFF with ZCS at both conditions. Figs. 14(d) and 15(d) show that diode D_2 is turned OFF with ZCS at both conditions. It is seen from experimental results that switch S_1 is turned ON and OFF with ZCS and diodes D_1 and D_2 are turned OFF with ZCS, respectively, due to the resonant components. Figs. 14(e) and 15(e) show the experimental waveforms of current i_{Cr} and voltage v_{Cr} which are also determined by resonant components. Figs. 14(f) and 15(f) show the experimental waveforms of output voltage v_o and doubler capacitor voltage v_{Cd}.

Fig. 16(a) shows the calculated, simulated, and experimental voltage gain curves of the proposed single switch converter. The calculated and simulated voltage gains are in close agreement with the experimental voltage gain. Fig. 16(b) shows the switching frequency fluctuation according to the output resistance value. The higher the voltage gain, the narrower the switching frequency fluctuation. Fig. 17 shows the efficiency curves of the proposed converter. The measured peak efficiencies of the proposed converter according to different input voltage 38 and 48 V are 96.55% and 96.98%, respectively. It should be noted that the efficiencies are greater than 95% at power levels above half-load at $V_i = 48$ V.

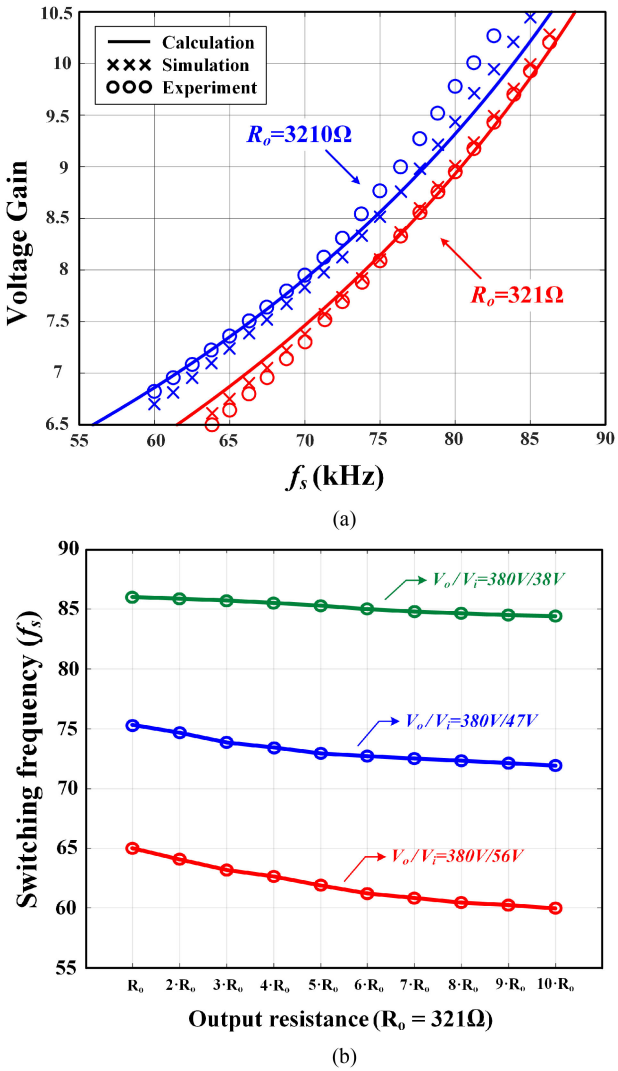

Fig. 16. (a) Calculated, simulated, and experimental voltage gains of the proposed converter at different R_o. (b) Switching frequency fluctuation according to output resistance.

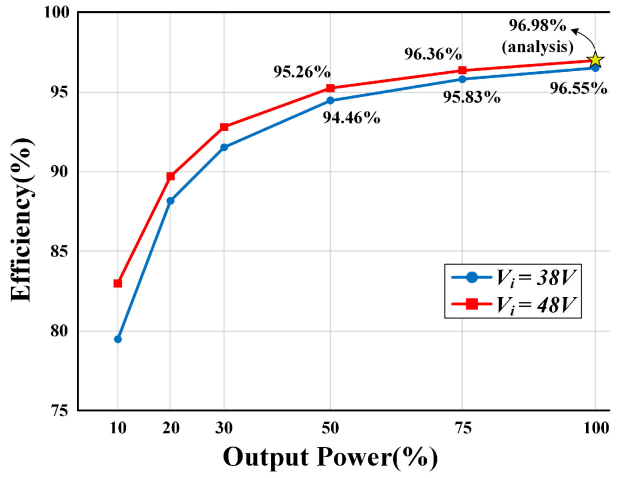

Fig. 17. Measured efficiency of proposed single switch converter.

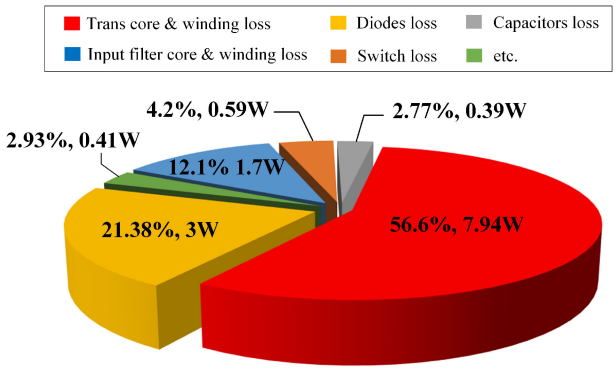

Fig. 18. Loss analysis of proposed topology when $V_i = 48$ V and $P_o = 450$ W operation condition.

Fig. 18 shows loss analysis of the proposed converter at full load when $V_i = 48$ V. The total loss of the proposed converter is 14.03 W. The large portion of the losses comes from transformer loss and diodes loss, which are 56.6% and 21.38% of the total loss, respectively.

VI. Conclusion

In this article, a single switch resonant converter is proposed for isolated high step-up application such as microconverter, portable fuel cell, uninterruptible power systems, and portable power station. The proposed converter has simple structure due to absence of clamp circuits. Zero dc-offset current of the transformer makes the transformer volume relatively small compared to the conventional flyback based single switch converter. Further, the proposed converter achieves ZCS turn-ON and turn-OFF of the switch and ZCS turn-OFF of all diodes regardless of input voltage and load variation. Experimental results from a 450-W prototype are provided to validate the proposed concept. The prototype converter achieved peak efficiency of 96.98% at 450-W full-load condition.

References

[1] X. Zhao, C. Chen, J. Lai, and O. Yu, "Circuit design considerations for reducing parasitic effects on GaN-based 1-MHz high-power-density high-step-up/down isolated resonant converters," *IEEE J. Emerg. Sel. Topics Power Electron.*, vol. 7, no. 2, pp. 695–705, Jun. 2019.

[2] C. Lim, Y. Jeong, and G. Moon, "Phase-shifted full-bridge DC–DC converter with high efficiency and high power density using center-tapped clamp circuit for battery charging in electric vehicles," *IEEE Trans. Power Electron.*, vol. 34, no. 11, pp. 10945–10959, Nov. 2019.

[3] M. Mousavi, Y. Sangsefidi, A. Mehrizi-Sani, and R. Beiranvand, "Generalized step-down switched-capacitor converter under ZCS for photovoltaic applications," *IEEE Trans. Energy Convers.*, vol. 33, no. 3, pp. 1321–1329, Sep. 2018.

[4] Z. Huang, Z. Liu, F. C. Lee, and Q. Li, "Critical-mode-based soft-switching modulation for high-frequency three-phase bidirectional AC–DC converters," *IEEE Trans. Power Electron.*, vol. 34, no. 4, pp. 3888–3898, Apr. 2019.

[5] H. F. Ahmed, H. Cha, A. A. Khan, and H. Kim, "A family of high-frequency isolated single-phase Z-source AC–AC converters with safe-commutation strategy," *IEEE Trans. Power Electron.*, vol. 31, no. 11, pp. 7522–7533, Nov. 2016.

[6] M. Pavlovsky, S. W. H. de Haan, and J. A. Ferreira, "Reaching high power density in multikilowatt DC–DC converters with galvanic isolation," *IEEE Trans. Power Electron.*, vol. 24, no. 3, pp. 603–612, Mar. 2009.

[7] M. Amirabadi, J. Baek, H. A. Toliyat, and W. C. Alexander, "Soft-switching AC-link three-phase AC–AC buck–boost converter," *IEEE Trans. Ind. Electron.*, vol. 62, no. 1, pp. 3–14, Jan. 2015.
[8] N. Soltau, D. Eggers, K. Hameyer, and R. W. De Doncker, "Iron losses in a medium-frequency transformer operated in a high-power DC–DC converter," *IEEE Trans. Magn.*, vol. 50, no. 2, pp. 953–956, Feb. 2014.
[9] D. A. Ruiz-Caballero and I. Barbi, "A new flyback-current-fed push-pull DC-DC converter," *IEEE Trans. Power Electron.*, vol. 14, no. 6, pp. 1056–1064, Nov. 1999.
[10] M. Nymand and M. A. E. Andersen, "High-efficiency isolated boost DC–DC converter for high-power low-voltage fuel-cell applications," *IEEE Trans. Ind. Electron.*, vol. 57, no. 2, pp. 505–514, Feb. 2010.
[11] F. J. Nome and I. Barbi, "A ZVS clamping mode-current-fed push-pull DC-DC converter," in *Proc. IEEE Int. Symp. Ind. Electron.*, 1998, pp. 617–621.
[12] Q. Wu, Q. Wang, J. Xu, and L. Xiao, "A wide load range ZVS push–pull DC/DC converter with active clamped," *IEEE Trans. Power Electron.*, vol. 32, no. 4, pp. 2865–2875, Apr. 2017.
[13] R. L. Andersen and I. Barbi, "A ZVS-PWM three-phase current-fed push–pull DC–DC converter," *IEEE Trans. Ind. Electron.*, vol. 60, no. 3, pp. 838–847, Mar. 2013.
[14] S. Han, H. Yoon, G. Moon, M. Youn, Y. Kim, and K. Lee, "A new active clamping zero-voltage switching PWM current-fed half-bridge converter," *IEEE Trans. Power Electron.*, vol. 20, no. 6, pp. 1271–1279, Nov. 2005.
[15] J. Kwon and B. Kwon, "High step-up active-clamp converter with input-current doubler and output-voltage doubler for fuel cell power systems," *IEEE Trans. Power Electron.*, vol. 24, no. 1, pp. 108–115, Jan. 2009.
[16] H. Kim, C. Yoon, and S. Choi, "An improved current-fed ZVS isolated boost converter for fuel cell applications," *IEEE Trans. Power Electron.*, vol. 25, no. 9, pp. 2357–2364, Sep. 2010.
[17] V. Yakushev, V. Meleshin, and S. Fraidlin, "Full-bridge isolated current fed converter with active clamp," in *Proc. 14th Annu. Appl. Power Electron. Conf. Expo.*, 1999, pp. 560–566.
[18] R. Watson and F. C. Lee, "A soft-switched, full-bridge boost converter employing an active-clamp circuit," in *Proc. Rec. 27th Annu. IEEE Power Electron. Specialists Conf.*, 1996, pp. 1948–1954.
[19] P. U. R and A. K. Rathore, "Extended range ZVS active-clamped current-fed full-bridge isolated DC/DC converter for fuel cell applications: Analysis, design, and experimental results," *IEEE Trans. Ind. Electron.*, vol. 60, no. 7, pp. 2661–2672, Jul. 2013.
[20] F. Evran and M. T. Aydemir, "Z-source-based isolated high step-up converter," *IET Power Electron.*, vol. 6, no. 1, pp. 117–124, Jan. 2013.
[21] J. Lee, T. Liang, and J. Chen, "Isolated coupled-inductor-integrated DC–DC converter with non-dissipative snubber for solar energy applications," *IEEE Trans. Ind. Electron.*, vol. 61, no. 7, pp. 3337–3348, Jul. 2014.
[22] J. Kwon, W. Choi, and B. Kwon, "Single-switch quasi-resonant converter," *IEEE Trans. Ind. Electron.*, vol. 56, no. 4, pp. 1158–1163, Apr. 2009.
[23] J. Lee, J. Park, and J. H. Jeon, "Series-connected forward–flyback converter for high step-up power conversion," *IEEE Trans. Power Electron.*, vol. 26, no. 12, pp. 3629–3641, Dec. 2011.
[24] A. Emrani, E. Adib, and H. Farzanehfard, "Single-switch soft-switched isolated DC–DC converter," *IEEE Trans. Power Electron.*, vol. 27, no. 4, pp. 1952–1957, Apr. 2012.
[25] J. Zeng, W. Qiao, and L. Qu, "LCL-resonant single-switch isolated DC–DC converter," *IET Power Electron.*, vol. 8, no. 7, pp. 1209–1216, 2015.
[26] S. Ryu, J. Ahn, B. Lee, and K. Cho, "Single-switch ZVZCS quasi-resonant CLL isolated DC-DC converter for low-power 32″ LCD tV," in *Proc. IEEE Energy Convers. Congr. Expo.*, 2013, pp. 4887–4893.
[27] K. Kanathipan, R. Emamalipour, and J. Lam, "A single-switch high-gain PV micro-converter with low-switch-voltage-to-high-voltage-bus ratio," *IEEE Trans. Power Electron.*, vol. 35, no. 9, pp. 9530–9540, Sep. 2020.
[28] J. Lee, M. Kim, H. Jeong, and S. Choi, "Single switch ZCS resonant converter with high step-up ratio," in *Proc. IEEE 8th Int. Power Electron. Motion Control Conf.*, 2016, pp. 3495–3500.
[29] J. Lee, M. Kim, and S. Choi, "A single switch ZCS parallel resonant converter with high step-up ratio," in *Proc. Annu. Conf. KIPE*, Jul. 2014, pp. 163–164.
[30] J. Lee, "A single switch ZCS parallel resonant converter with high Step-up ratio," Master dissertation, Dept. Electrical and information Eng., Seoul Nat. Univ. Sci. Technol., Seoul, South Korea, 2015.
[31] M. Kim and S. Choi, "A fully soft-switched single switch isolated DC–DC converter," *IEEE Trans. Power Electron.*, vol. 30, no. 9, pp. 4883–4890, Sep. 2015.
[32] D. Sha, J. Zhang, and J. Wu, "A GaN-based micro-converter utilizing fixed-frequency BCM control method for PV applications," *IEEE Trans. Ind. Electron.*, vol. 65, no. 6, pp. 4771–4780, Jun. 2018.
[33] Y. Qu, W. Shu, and J. Chang, "A fully soft switched point-of-load converter for resource constraint drone applications," *IEEE Trans. Power Electron.*, vol. 35, no. 3, pp. 2705–2713, Mar. 2020.
[34] Y. Qu and Z. Wang, "Soft-switching techniques for single-inductor multiple-output LED drivers," *IEEE Trans. Power Electron.*, vol. 35, no. 12, pp. 13748–13756, Dec. 2020.
[35] Y. Qu, W. Shu, L. Qiu, Y. Kuan, S. Chiang, and J. Chang, "A low-profile high-efficiency fast battery charger with unifiable constant-current and constant-voltage regulation," *IEEE Trans. Circuits Syst. I, Regular Papers*, vol. 67, no. 11, pp. 4099–4109, Nov. 2020.

Jaeyeon Lee was born in South Korea, in 1991. He received the B.S. and M.S. degrees in 2014 and 2016, respectively, from the Department of Electrical and Information Engineering, Seoul National University of Science and Technology (Seoul Tech), Seoul, South Korea, where he is currently working toward the Ph.D. degree in electrical and information engineering.

From 2016 to 2019, he was a Research Engineer with Dasstech Co., Ltd., Cheongju, South Korea. His research interests include power conversion technologies for renewable energy system and battery chargers for electrical vehicles.

Minjae Kim received the B.S., M.S., and Ph.D. degrees in new energy engineering from Seoul National University of Science and Technology (Seoul Tech), Seoul, South Korea, in 2011, 2013, and 2016, respectively.

In 2017, he joined the New Power Plasma Co., Ltd., Pyeongtaek, South Korea. His research interests include power conversion technologies for renewable energy system and remote plasma source.

Sunju Kim was born in South Korea, in 1994. He received the B.S. and M.S. degrees in 2017 and 2019, respectively, from the Department of Electrical and Information Engineering, Seoul National University of Science and Technology (Seoul Tech), Seoul, South Korea, where he is currently working toward the Ph.D. degree in electrical and information engineering.

His research interests include power conversion technologies for renewable energy system and battery chargers for electrical vehicles.

Sewan Choi (Fellow, IEEE) received the Ph.D. degree in electrical engineering from Texas A&M University, College Station, TX, USA, in 1995.

From 1985 to 1990, he was with Daewoo Heavy Industries as a Research Engineer. From 1996 to 1997, he was a Principal Research Engineer with Samsung Electro-Mechanics Co., South Korea. In 1997, he joined the Department of Electrical and Information Engineering, Seoul National University of Science and Technology (Seoul Tech), Seoul, South Korea, where he is currently a Professor. His research interests include power conversion technologies for renewable energy systems and dc -dc converters and battery chargers for electric vehicles.

Dr. Choi has been serving as an Associate Editor of the IEEE TRANSACTIONS ON POWER ELECTRONICS since 2006. He is President of Korean Institute of Power Electronics in 2021. He was TPC Chair of ICPE2019-IEEE ECCE Asia held in Busan, Korea. He is currently serving as Chairman of IEEE PELS Seoul section.